Agriculture, Forestry and Fisheries
2014; 3(6-1): 36-45
Published online November 17, 2014 (http://www.sciencepublishinggroup.com/j/aff)
doi: 10.11648/j.aff.s.2014030601.16
ISSN: 2328-563X (Print); ISSN:2328-5648 (Online)

Evapotranspiration and water stress estimation from TIR and SWIR bands

Girolimetto Daniela, Venturini Virginia

Centro de Estudios Hidro Ambientales, Facultad de Ingeniería y Ciencias Hídricas, Universidad Nacional del Litoral, C. C. 217, Santa Fe, (3000) Argentina

Email address:
dgirolimetto@fich.unl.edu.ar (G. Daniela), vventurini@fich.unl.edu.ar (V. Virginia)

To cite this article:
Girolimetto Daniela, Venturini Virginia. Evapotranspiration and Water Stress Estimation from TIR and SWIR Bands. *Agriculture, Forestry and Fisheries.* Special Issue: Agriculture Ecosystems and Environment. Vol. 3, No. 6-1, 2014, pp. 36-45.
doi: 10.11648/j.aff.s.2014030601.16

Abstract: The World agriculture depends on water availability; thus, a successful water management system would assure food for the World. For several decades, the scientific community has developed methods to support water management. These models include the estimates of the main water loss in the system, i.e. the evapotranspiration (ET). In turn, the satellite technology encouraged the development of new models to monitor large regions. In this work, we present a modified ET estimation adapting the F parameter introduced by Venturini et al., in 2008. Additionally, a new simple index to estimate water stress (WS) for different types of surfaces, is also presented. The relative evaporation represented by F is derived from the soil moisture condition following the formulation of Barton and computed from the surface reflectance in the shortwave infrared bands (SWIR). The new ET and WS equations are applicable, with different satellite datasets, to any remote region since they are based on universal relationships. The preliminary results show errors of about 11% in ET. In general, the new WS index would have values of approximately 0.8 for a dry surface and 0.4 for a wet surface.

Keywords: Evapotranspiration, Water Stress, Remote Sensing, TIR, SWIR

1. Introduction

The evapotranspiration (ET) is the most significant water withdrawal in the water balance. Therefore, in recent years, the scientific community has given special attention to the ET impact on global circulation models and has devoted efforts to estimate how much water is globally evaporating [1]. Even today, a precise ET calculation is a real challenge for water resources practitioners. Moreover, the need to monitor large regions has motivated the development of new methods for calculating ET from remote sensing data. Thus, diverse ET models have been developed and widely applied with varying results [e.g. 2-8]. The importance of ET in the global water balance was remarked by the satellite mission Aquarius/SAC-D, a cooperation program between the NASA and Argentina. This mission seeks to determine how the ocean responds to the combined effects of evaporation, precipitation, ice melt and river runoff, in order to analyze their impact on the global water distribution as well as the global freshwater availability (http://aquarius.nasa.gov/).

The world agriculture depends on the availability of water, being the water management one of the main components of the success or failure of modern agriculture. Thus, indices to determine water stress (WS) of vegetation have been widely used to assist farmers in maximizing production. Many of them have been developed using remotely sensed data, allowing the WS estimation in large regions to be made [9-13]. For instance, Moran et al., [9] published a definition of WS in terms of latent heat fluxes, which can be expressed as $WS=1-(ET/E_{pot})$, where E_{pot} is the potential evapotranspiration and the ratio ET/E_{pot} is the relative evaporation. This formulation emphasizes the importance of an accurate ET calculation, not only for water management systems and risks but also for the agriculture and related food industries.

Even though there is a large set of ET models, we focussed on Venturini et al.'s method [8] because it presents interesting advantages. The authors presented a new formulation to derive ET maps from remotely sensed data without applying auxiliary or site-specific relationships. The method was based on Granger's complementary relationship and Priestley–Taylor equation to eliminate the wind function

and the resistance parameters, by including the relative evaporation concept (F). The method was applied in different environments with errors of about 15% from the mean ET and proved to be better than similar ET models [14].

In this paper, we propose a simple methodology that relates the F concept to the surface moisture availability concept defined by Barton [15]. This new calculation exploits the water absorption properties of the SWIR region. The SWIR energy is absorbed by water; therefore, these bands are sensitive to the surface moisture content variations [16] and had been related to the concept of relative humidity of a surface. This new F concept is used in Venturini et al.'s method to compute ET and to derive a new WS index.

2. Methodologies

In this session, Venturini et al.'s method is briefly presented before the rationale behind the F parameter, and the new WS index is introduced.

2.1. Venturini et al.'s Method

Venturini et al., modified the Priestley–Taylor (P-T) model [17] using Granger's complementary relationship [18] and the relative evaporation, defined as the ratio between ET and E_{pot}. The relative evaporation proposed by Granger and Gray [3] was used for defining a coefficient F, assuming that the wind function affects ET and E_{pot} in a similar way. The authors also assumed that saturation and actual vapor pressures can be calculated from the saturation vapor pressure curve (SVP) with temperature data. Thus, $F=ET/E_{pot}$ can be expressed as

$$F = \frac{ET}{E_{pot}} = \frac{e_{s_u} - e_a}{e_s^* - e_a} \cong \frac{(T_u - T_d)\Delta_1}{(T_s - T_d)\Delta_2} \quad (1)$$

where e_s is the surface actual water vapor pressure, e^*_s is the surface saturation water vapor pressure, e_a is the air actual water vapor pressure, T_s is the surface temperature and T_u is the temperature of the surface if it is brought to saturation without changing the actual surface vapor pressure, which is analogous to the dew point temperature (T_d) definition [8]. Therefore, E_{pot}= ET/F (see equation 1) combined with Granger´s complementary equation renders ET as a function of the wet environment evapotranspiration (E_w), as follows,

$$ET = E_w \frac{F(\Delta + \gamma)}{F\Delta + \gamma} \quad (2)$$

where γ is the psychrometric constant, Δ is the slope of the SVP curve, and E_w is the wet environment evapotranspiration.

The Priestley and Taylor equation [17] was used to compute E_w. Consequently, by combining the Priestley–Taylor expression with equations (2) and (1), the following model (hereinafter named as $ET_{V\text{-}V}$) was derived

$$ET_{V-V} = \alpha \frac{F\Delta}{F\Delta + \gamma}(R_n - G) \quad (3)$$

where α is a P-T parameter, assumed to be equal to 1.26 for saturated surfaces, R_n is the net radiation, and G is the soil heat flux.

The new variable introduced in this formulation, T_u, is necessary to determine e_s and then F (see equation 1). The authors determined T_u from the SVP curve using T_s and T_d (see Figure 1); however, they recognize that the T_u calculation did not follow the physics of the problem [19]. A full discussion regarding the definition and calculation of T_u can be found in [8] and [19].

Once T_u is estimated, e_s can be computed, and then F and ET can be calculated.

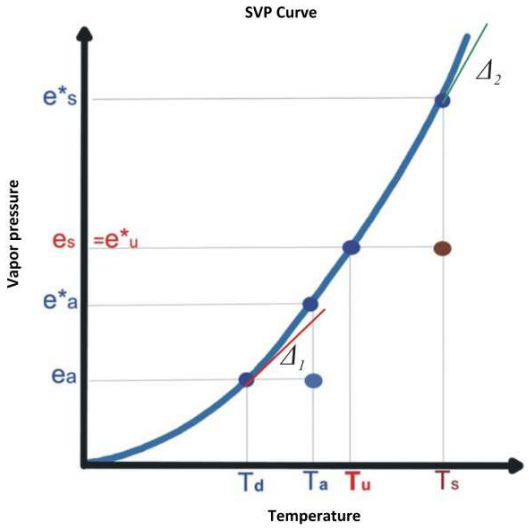

Figure 1. *SVP curve T_u, T_s, e_s, e^*_s relationship in de T_s context.*

2.2. The New Method to Estimate e_s

The e_s estimation could be enhanced by using a surface variable, such as the surface moisture content. The new e_s calculation involves the surface water availability proposed by Barton [15], as follows:

$$\sigma = \frac{e_a}{e_s^*} \quad (4)$$

where σ is an indicator of the near surface moisture availability [15].

Barton analyzed the ground evaporation data in terms of σ that is directly related to the soil moisture (SM) content. Hence, the author empirically related σ to the bare SM data for the Deniliquin (Australia) region that are calculated with data from active microwave sensors. The author proposed the following relationship:

$$\sigma = \frac{1.8SM}{SM + 30} \quad SM < 37.5 \quad (5)$$

$$\sigma = 1 \quad SM > 37.5 \quad (6)$$

where SM is the soil moisture content (in percentage).

Deniliquin is a semi-arid region where the bare soil surface saturates with moisture contents higher than 37.5%. The soil is clayey with a patchy vegetation pattern dominated by mesophytic species forming a relatively dense sward. In this region, the mean annual rainfall and evaporation amount to 40 cm and 161 cm respectively and the mean temperature varies from 40 ºC in July and 24 ºC in January. Therefore, equations (5) and (6) were derived from site-specific relationships and were difficult to extrapolate to other areas. Barton derived σ for bare soil surfaces and it is not evident how it varies for mixed soil-vegetation. Nevertheless, Barton stated that this parameterization is convenient because it can be simply incorporated in an ET model and that the formulation would not need the determination of either the surface temperature or the nature of the surface.

From the remote sensing point of view, the SWIR energy is absorbed by water; therefore, these bands are sensitive to the surface moisture content variations [16]. Many authors combined the NIR and SWIR reflectance to study changes in foliar water content [20-27, 16, 28-29]. Fensholt and Sandholt in 2003 [24] explained that even though the atmosphere, the leaf/surface internal structure and the dry matter content might affect the vegetation SWIR reflectance, their effects are negligible compared with water absorption. Simulations of the leaf reflectance of SWIR bands showed that over 50% of the changes in reflectance of the SWIR region are due to the absorption caused by the water content in the vegetation [30].

The strong water absorption occurring at wavelengths > 1.0 μm makes the mix surface moisture the main cause for the SWIR variation. Thus, the SWIR reflectances of the soil and vegetation are negatively related to the moisture [26, 31]. Consequently, considering the surface as a vegetation-soil complex and assuming that the decrease of the reflectance in the SWIR is essentially due to the water content of the surface, we approximate σ as:

$$\sigma = \frac{Rsat}{Ri} \tag{7}$$

where Rsat is the SWIR reflectance of a saturated surface and Ri is the SWIR reflectance of any i^{th}-pixel.

Rsat is easily obtainable from the relation between Ri and SM, where ground data are available. Otherwise, it can be calculated from the mean Ri of the pixels identified as water in an image. In any case, the values of Ri close to zero would be associated to saturated pixels and can be considered as Rsat. This point is further explained in session 4.

If Rsat is known, it is possible to obtain σ and apply equation (4) to estimate e_s (e_s=σe^*_s). Introducing e_s in equation (1),

$$F = \frac{\sigma e_s^* - e_a}{e_s^* - e_a} \tag{8}$$

Thus, ET is estimated from equation (3) with the new F that incorporates the physically consistent T_u estimation.

2.3. New Water Stress Index WSIF

ET is commonly used to index the vegetation stress, as well as to estimate the volume of water needed for irrigation. We used the new ET model in a water stress index, following Moran et al.'s concepts [9].

Moran et al. discussed the validity of the CWSI theory for partially vegetated areas. They derived an index based on the interpretation of the trapezoidal shaped IV-(T_s-T_a) plot, where T_a is the air temperature.

The WDI ponders two important assumptions associated to the relationship between IV and the difference T_s-T_a. The authors assume that the difference T_s-T_a is linearly related to the percentage of vegetated area and to the canopy and soil temperatures. Another important statement made by Moran et al. is that, given a certain net energy (R_n), the temperatures of the foliage and soil are linearly related to the transpiration and evaporation respectively. Therefore, the variations in T_s-T_a would be associated to ET and (for a partially vegetated area) WDI is:

$$WDI = 1 - \frac{ET}{E_{pot}} \tag{9}$$

where (ET/E_{pot}) is the relative evaporation.

Thus, it is possible to rewrite Moran et al.'s formulation replacing ET/E_{pot} by F (see equation 1), as follows:

$$WSI_F = 1 - F = 1 - \frac{(e_s - e_a)}{(e_s^* - e_a)} = \frac{(e_s^* - e_a)}{(e_s^* - e_a)} \tag{10}$$

Knowing that $e_s = \sigma e^*_s$, with σ determined from the SWIR reflectance (see equation 4), WSI_F can be re-written as follows,

Alpha

$$WSI_F = \frac{(e_s^* - e_s)}{(e_s^* - e_a)} = \frac{(e_s^* - \sigma e_s^*)}{(e_s^* - e_a)} \tag{11}$$

The new index tends to zero when σ tends to 1, i.e. for a saturated area, e_s tends to the saturation vapor pressure (e^*_s) [see Figure 1 and equation (11)]; therefore, WSI_F would tend to zero indicating the non-stress condition. On the contrary, when σ tends to zero, e_s=σ*e^*_s tends to e_a [see Figure 1 and equation (11)] and WSI_F would be close to 1, reflecting a full stress condition.

3. Study Area and Data

3.1. Study Area

The Southern Great Plain (SGP) region extends over the State of Oklahoma and southern part of Kansas, running from longitude 95.5º W to 99.5º W and from latitude 34.5º N to 38.5º N. It is a flat terrain, with heterogeneous land cover and a wide variety of weather throughout the year. Winters are very cold and summers are very hot and humid. The prairies support abundant wildlife.

This region has a relatively extensive and well distributed coverage of ground Energy Fluxes and Bowen stations, maintained by the Atmospheric Radiation Measurement (ARM) program (http://www.arm.gov). The stations are widely distributed over the whole domain (Figure 2). The sites are named according to the instruments located in each facility and numbered sequentially as each new center is opened; for example, "E5" refers to the extended facility site number 5. Extended facility instruments include an Energy Balance Bowen Ratio system (EBBR), which produces 30 minute estimates of the vertical fluxes of sensible and latent heat at the local surface.

In this work, we used data from the following stations: station E8 and E22, located in a grazed rangeland region; E4, located in an ungrazed rangeland area; E13, located in a region with pasture and wheat; E7, E9, E15, E20 and E27, located in pastures; E18 and E19 located in an ungrazed pasture area; E12, located in a native prairie; E10 located in an alfalfa region; E16 located in a wheat region; and E2 located in a grass region.

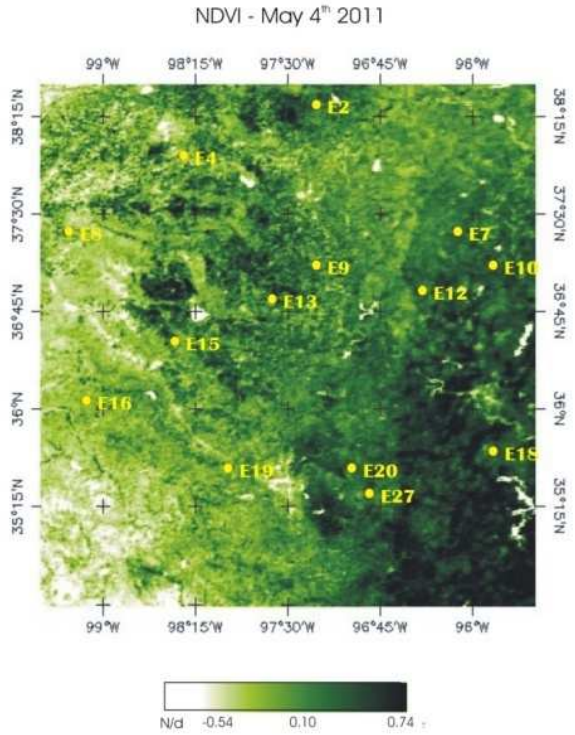

Figure 2. *Southern Great Plains Region and ground station locations.*

3.2. Data and Image

The Energy Balance Bowen Ratio (EBBR) system computes 30-min estimates of the sensible and latent heat vertical fluxes at the local scale. The fluxes from the EBBR stations are calculated with observations of R_n, G, and the vertical gradients of temperature and relative humidity (RH). The instruments and measurement applications are well established and have been used for validation purposes in many studies [32-33, 8, 34]. Further information about the ARM EBBR data and methodology is available at http://www.arm.gov

The imageries used in this work were registered by the MODIS sensor. MODIS is one of the instruments on board EOS-Terra and EOS-Aqua satellites [http://modis.gsfc.nasa.gov/, 35-36].

Daytime MODIS-Aqua images for nine days during spring and summer, with at least 80% of the study area free of clouds, were selected. Table 1 summarizes the image information, including date, day of the year, satellite overpass time and image quality. MYD02, MYD07 and MYD11 were the three products needed for this application.

The MYD02 has corrected radiance, reflectance and geolocations for 36 bands at 1x1 km. The MODIS Atmospheric profile (MOD07) offers several parameters. Air temperature (T_a) and T_d profiles were used in the current study. The spatial resolution of this daily product is 5×5 km^2 at 20 vertical atmospheric pressure levels [37]. This product was already used in a similar work by Bisht et al.'s [38] and Venturini et al.'s [8, 19]. Bisht et al.'s analyzed the agreement between MOD07 and T_a and observed T_a in the SGP, concluding that MOD07 is a good surrogate of field observations of T_a. The MYD11 product supplies T_s images on a daily basis [39, 40, 19].

Table 1. *Date, day of the year, overpass time and image quality of the nine study days*

Date	Day of the year (DOY)	Overpass time (UTC)	Image quality (% clouds)
April 6th 2011	96	19:30	15
May 4th 2011	124	19:55	1
May 26th 2011	146	19:20	2
May 29th 2011	149	19:50	1
June 5th 2011	156	19:55	14
April 10th 2010	100	19:40	5
June 4th 2010	155	19:45	18

4. Results

4.1. Preprocessing

The MODIS images were georeferenced from the latitude and longitude provided in each product. T_a and T_d images corresponded to the vertical pressure level of 950 hPa, the profile closer to the surface in MYD07. It is worth mentioning that T_a and T_d are assumed to be homogenous over the area of 5 km^2 [37], while T_s from the MYD11 product is provided in pixels of 1 km^2. The study area was pulled out of each image and projected on a grid of 445 columns by 445 rows, with a resolution of approximately 1 km per pixel.

The images of the SWIR band at 2130 nm (R7) were used to approximate σ. R7 was previously corrected for atmospheric effects following the dark object method [41].

e^*_s and e_a were estimated with Buck´s equation [42], using the T_s and T_d images respectively. Finally, ET and WSI_F were computed for the SGP region.

4.2. Analysis of σ

The Rsat parameter must be estimated to obtain σ from equation (4). In this work, Rsat was attained from R7 and SM ground data, in gravimetric percentage.

EBBR-SM data at 5 cm were selected because they were the nearest to the surface. Figure 3 shows the relationship between SM data and the R7 of the pixel where the EBRR station is located. These data indicate that R7 turns out to be asymptotic at 0.06 for SM values greater than 25%, suggesting the saturation condition of the surface for this region.

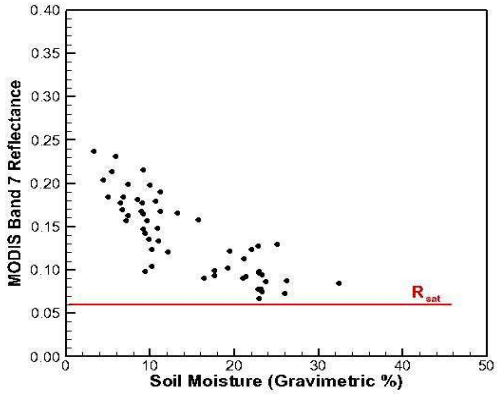

Figure 3. *Ri versus soil moisture (gravimetric %) plot where Rsat limit is indicated.*

This value is consistent with the regional water reflectance (RWR) in the SWIR band (Table 2) obtained as $RWR=(\sum R_d^{water})/n$, where R_d^{water} is the mean reflectance of the pixels identified as water (NDVI <0) in the SWIR band on a given day, and n is the total of the days analyzed.

Table 2. *Water reflectance in the SWIR band for each day analyzed and RWR.*

Date	R_d^{water}
April 6th 2011	0.049
May 4th 2011	0.044
May 26th 2011	0.082
May 29th 2011	0.034
June 5th 2011	0.095
April 10th 2010	0.052
June 4th 2010	0.065
$RWR=(\sum R_d^{water})/n$	0.059

Table 3. *Regional Minimum, Mean and Standard deviation of σ.*

Date	Min	Mean	Standard deviation
April 6th 2011	0.15	0.40	0.077
May 4th 2011	0.16	0.37	0.098
May 26th 2011	0.20	0.55	0.178
May 29th 2011	0.16	0.40	0.132
June 5th 2011	0.14	0.38	0.140
April 10th 2010	0.17	0.41	0.076
June 4th 2010	0.17	0.44	0.112
June 5th 2009	0.22	0.58	0.150
August 22th 2009	0.18	0.59	0.171

Then, σ was obtained for each of the days tested with Rsat and R7 of each pixel for each selected day.

The regional statistics of σ (means, minimums and standard deviation) are shown in Table 3.

The maximum σ value is approximately equal to 1 for all the days studied, which suggests that there were saturated pixels during the studied period. The minimum σ value varies from 0.14 to 0.22, indicating that there may be pixels with little SM. In general, the σ regional mean value is larger than 0.4, indicating that the region is drying; the standard deviations vary from 0.076 to 0.178, which is consistent with different degrees of dispersion around the mean.

Barton [15] did not reported values of σ for mixed soil-vegetation surfaces because σ is difficult to assess in mixed surfaces. Thus, we had to establish a criterium for the saturation condition of a soil+vegetation pixel. Hence, we assumed that a value of SM greater than 25% represents the saturation limit for a mixed surface and that σ values greater than 0.70 would indicate a saturated surface. It is worth noting that these limits may vary with the soil and vegetation type and that the index range interpretation may vary from region to region.

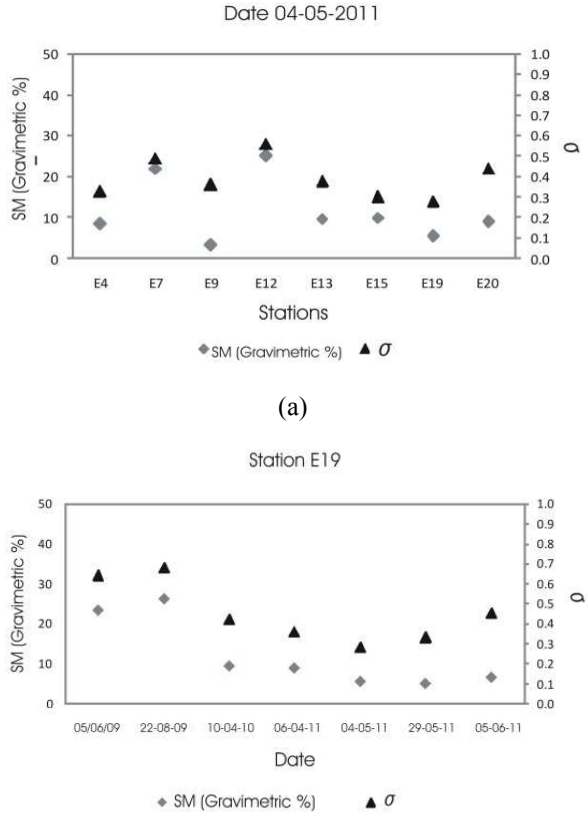

Figure 4. *(a) σ* versus *soil moisture (SM) for day 04/05/2011 and (b) σ* versus *SM for station E19.*

The results obtained on 04/05/2011, with only 1% of cloud cover, were selected to exemplify the general regional variations. Figure 4(a) shows the areal distribution of SM

and σ for the day 04/05/2011, where a good general agreement is observed. Station E19 was selected to exemplify the time variation because the data were available in 80% of the days analyzed. Figure 4(b) displays a temporal variation of SM and σ for station E19. Both variables (σ and SM) seem to follow the same variation over time, although SM is a point measurement and σ is the response of a mixed pixel of approximately 1 km^2.

4.3. Validation of ET Modified from σ (ET_{G-V})

The ET estimates ($ET_{modeled}$) computed from Venturini et al.'s original and modified equations were contrasted with observed ET (ET_{ground}). The validation procedure presented in this session was widely used in others works [4, 43, 5, 38, 44, 8, 19].

The regional maximum, minimum and average ET values are shown in Table 4; clearly, ET_{V-V} and ET_{G-V} methods yielded similar results. The mean ET ground data differs from the mean ET models in 13.10 Wm^{-2} and -14.69 Wm^{-2} for ET_{V-V} and ET_{G-V} respectively. While ET_{V-V} overestimates the ET, ET_{G-V} underestimates the regional observed ET from field measurements. However, these differences are comparable to those presented by other authors [43-44, 8].

Table 4. *Overall Maximum, Minimum and Mean* ETv-v, ET_{G-V} *and* ET_{ground} *for 54 sample pixels.*

ET model	Max (Wm^{-2})	Min (Wm^{-2})	Mean (Wm^{-2})
ET_{ground}	544.63	180.18	350.62
ET_{V-V}	478.97	196.63	363.72
ET_{G-V}	492.91	185.48	335.93

The bias, the root mean square error (RMSE) and the correlation coefficient (r) were used to analyze the soundness of the new model. The bias was calculated as $[\sum(ET_{ground}-ET_{modeled})]/n_{obs}$ and the RMSE as $[\sum(ET_{ground}-ET_{modeled})^2/n_{obs}]^{0.5}$, where n_{obs} is the number of observations (54 points). The ET_{V-V} method presented a RMSE of approximately 19% from the observed ET values. The bias was 4%. The ET_{G-V} methodology yielded a RMSE of 39.92 Wm^{-2} and -14.69 Wm^{-2} for the bias, which represent 11% and 4% from the observed mean ET respectively. The correlations were r =0.92 for ET_{G-V} and r=0.74 for ET_{V-V}.

The ET_{G-V} model would imply a significant improvement in ET estimates with remotely sensed data. For instance, Venturini et al.'s in 2008 [8] published values for the RMSE and the bias of about 18% and 15% from the observed mean ET for the same region. Kalma et al.'s [45] conducted a thorough analysis where results from about 30 published ET validation studies were summarized. These authors reported RMSE values of about 50Wm^{-2} and relative errors of about 15 to 30%. Long and Singh [46] recently published RMSEs of 45.6 Wm^{-2} and 63.1 Wm^{-2} using Landsat TM/ETM+ and ASTER images respectively.

Table 5 shows the RMSE and the bias for each analyzed day for ET_{V-V} and ET_{G-V} models. In general, the RMSEs for the ET_{G-V} model are lower than 13% from the mean ET of each day; the biases are up to 8% from the observed mean ET. Only the day 04/06/2010 presented a RMSE of 18% with a bias of the same order. The quality of the image of day 04/06/2010 is not very good and few stations are free of clouds, which may cause uncertainties in the imagery. The ET_{V-V} method presents RMSE maximum values of approximately 30% from the observed ET mean.

These preliminary results suggest that the ET_{G-V} model correlates better with the measurements than the ET_{V-V} model.

The state of the surface moisture introduced by σ is consistent with the T_u and e_s definition; consequently, σ improves the results of the ET_{V-V} model. The new ET_{G-V} method yields precise ET estimates while it is simple to apply with remotely sensed data and easily coded for routinary applications without the user supervision.

Table 5. *ET (Wm^{-2}) comparison between observations and proposed method estimates for each day analyzed and the global RMSE and bias during the study period.*

Date	# of obs.	ET_{V-V}		ET_{G-V}	
		RMSE	Bias	RMSE	Bias
April 6th 2011	6	96.52	28.74	44.34	23.07
May 4th 2011	6	98.84	70.95	36.03	-23.83
May 26th 2011	4	20.95	10.84	16.97	7.01
May 29th 2011	6	70.63	3.54	39.15	-23.77
June 5th 2011	8	55.42	24.16	36.78	-18.82
April 10th 2010	5	44.67	42.42	29.63	-8.75
June 4th 2010	4	51.69	-19.97	84.05	-74.97
June 5th 2009	8	65.95	-24.67	31.53	-19.95
August 22th 2009	7	34.24	-11.94	25.85	-2.92
Global RMSE and bias	54	65.89	-13.10	39.92	14.69

4.4. WSI_F Results

Knowing that ET_{G-V} improves the ET estimates, we then tested the new WSI_F presented in equation (11).

The WSI_F regional average values are greater than 0.50 in all dates analyzed, suggesting that the region is within a moderately stressed period. These results are comparable with those found by Girolimetto and Venturini in 2013 [13], who estimated water stress from the NDVI-T_s plot in the same region and days analyzed. The WSI_F standard deviation value varies between 0.097 and 0.234, which is consistent with different degrees of dispersion around the

mean and different regional surface moisture distributions.

Since WS is not directly measurable, a validation strategy was needed. Thus, ground values, X_{obs}, were obtained as 1-(ET_{obs}/E_{pot_Samani}) and 1-($ET_{obs}/E_{pot\_Makkink}$). The RMSE was calculated as $[\Sigma(X_{obs}-WSI_F)^2/n]^{0.5}$. Samani [47] and Makkink's equations [48] were chosen for their simplicity and little field data requirement. The difference between 1-(ET_{obs}/E_{pot_Samani}) and WSI_F showed a bias of -0.046 and a RMSE of 0.094, which represents 19% from the mean value of WS. Comparison between 1-($ET_{obs}/E_{pot\_Makkink}$) and WSI_F showed a bias and a RMSE of -0.083 and 0.120 respectively, consistent with Colaizzi et al.'s results [10]. In all cases, the RMSEs are of the same order, indicating that errors of the methods are about 25-30% from the average WS.

WSI_F was also contrasted with observations of the SM, soil temperature (T_{soil}), precipitation of the previous 5 days (PP) and ET_{obs} to analyze the sensitivity of the index to capture different surface conditions. The relationship between the WSI_F and SM observations (at 5 cm from the surface) is shown in Figure 5. The relationship presented a correlation coefficient of 0.80 with the set of data available. This value is consistent with those published by other authors [49,24].

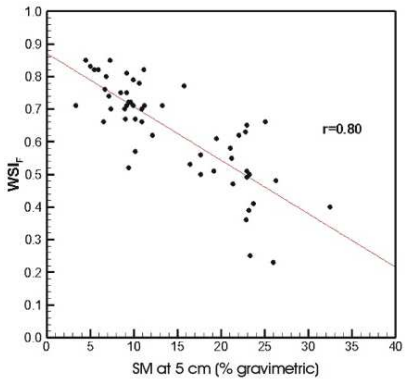

Figure 5. *WSI_F and SM ground observations relationship.*

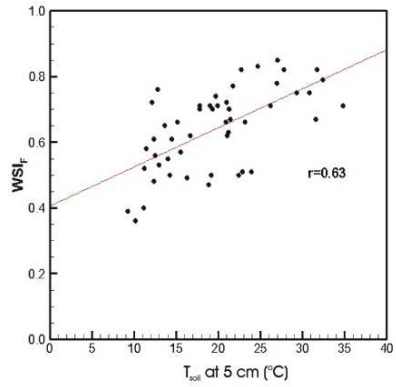

Figure 6. *WSI_F and SM and T_{soil} observations relationship.*

The relation between WSI_F and T_{soil} at 5 cm (Figure 6) yielded r=0.63. The soil temperature and WS vary with the soil water content, i.e. when the water content in soil decreases, WS and T_{soil} increase.

The relationship between PP and WSI_F shown in Figure 7 presents an r of 0.84, indicating that WSI_F is sensitive to variations in PP.

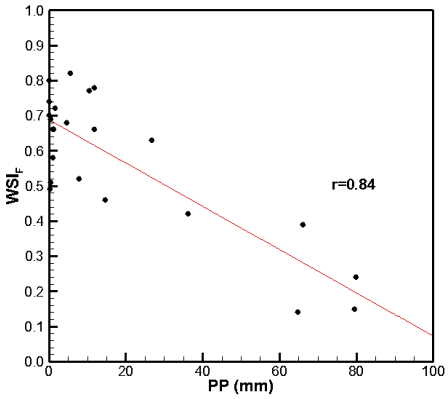

Figure 7. *WSI_F and PP observations relationship.*

Finally, the relationship between WSI_F and ET_{obs} presented in Figure 8 yielded a correlation of 0.71. The new index has a well-defined inverse relationship with ET_{obs} in the study area. WSI_F values of about 0.8 are related to values of ET of about 200 Wm^{-2}, while unstressed surfaces (WSI_F ~ 0.3) evapotranspire at a rate of 500-600 Wm^{-2}.

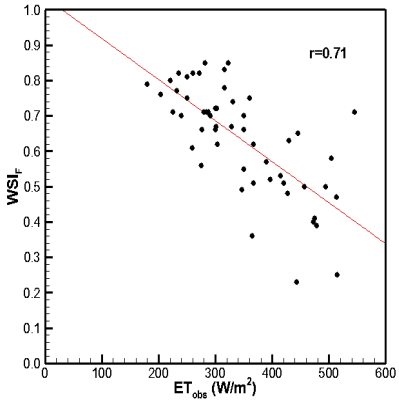

Figure 8. *WSI_F and ET_{obs} relationship*

5. Summary and Conclusion

In this paper, we propose a new simple methodology to obtain the relative evaporation parameter (F) introduced by Venturini et al. in 2008. This new F is derived from the soil moisture σ parameter defined by Barton [15] as e_s/e^*_s, which in turn can be obtained from the surface reflectance in the SWIR bands. SWIR energy is absorbed by water; therefore, these bands are basically sensitive to variations in moisture content of a surface, although there are other factors that might affect the band response. Physically speaking, e_s and the reflectance are inversely proportional to the surface moisture; accordingly, we propose to obtain σ as the relationship between the reflectance in the SWIR of the saturated pixel (Rsat) and the reflectance of the pixel i (Ri). Rsat can be estimated from the Ri *vs* SM curve or from the average value of the pixels identified with NDVI < 0. In any case, Rsat would tend to the minimum minimonum of R7.

The spatial and temporal analysis showed that the σ variation represents the SM data despite the different scales of observation and the pixel size. SM observations are valid for a few centimeters, the moisture being measured below the soil surface, and σ is the response of a mixed pixel of approximately 1 km^2.

As mentioned, σ enhanced the methodology to obtain the main parameter of Venturini et al.'s method. ET_{G-V} was compared with ET observed values and ET_{V-V} results. Even though this comparison is not exhaustive, results indicate that ET_{V-V} overestimates the ET_{obs}, while ET_{G-V} underestimates the $ET_{obs.}$.

The WSI_F derived from σ is based on the water vapor pressure gradient, combining the effects of surface moisture and temperature with those of the air, reflecting the stress caused by atmospheric conditions and surface parameters. In fact, considering the soil-plant-atmosphere complex system as a continuous, the soil face should be considered as a reservoir that supplies water to the system. Thus, any deficit that occurs in the reservoir adversely affects the system performance. In such a case, the physical stress process involves surface and atmospheric demands.

The WSI_F contrast with different WS indicators yields results similar to those published in other works. WSI_F is sensitive to SM and PP, and represents the rate of ET. We emphasize that SM, ET and PP observations are completely independent from the WSI_F.

The relationship between WSI_F and SM (R^2=0.8) provided information about the index limits. For instance, a soil with 5% of moisture matches a WSI_F of about 0.8 and a SM of 30% agrees with a WSI_F of about 0.3. The WSI_F would get close to 0 for surfaces with 25-30% of water, which represents a saturation point for most of the soils.

The main advantage of ET_{G-V} and WSI_F is that they are based on universal relationships. Although Rsat is a local parameter that would depend on the soil and vegetation type, it can be obtained from the reflectance of SWIR bands of each analyzed scene. This advantage renders the ET and WSIF equations applicable with different satellite missions and any remote region. ET_{G-V} and WSI_F required little processing of satellite images, resulting convenient for end users who require quick and easy to apply methods.

References

[1] R.K. Vinukollu, E.F. Wood, C.R. Ferguson and J.B. Fisher, "Global estimates of evapotranspiration for climate studies using multi-sensor remote sensing data: Evaluation of three process-based approaches", Remote Sensing of Environment, 2011, vol. 111, pp. 801-823.

[2] R.D. Jackson, R.G. Reginato and S.B. Idso, "Wheat canopy temperature: A practical tool for evaluating water requirements", Water Resources Research, 1977, vol. 13, pp. 651-656.

[3] R.J. Granger, and D.M. Gray, "Evaporation from natural nonsaturated surfaces", Journal of Hydrology, 1989, vol. 111, pp. 21-29.

[4] L. Jiang and S. Islam, "Estimation of surface evaporation map over southern Great Plains using remote sensing data", Water Resources Research, 2001, vol. 37, Issue 2, pp. 329-340.

[5] K. Nishida, R.R. Nemani, S.W. Running and J.M Glassy, "An operational remote sensing algorithm of land evaporation", Journal of Geophysical Research, 2003, vol. 108, No. D9, pp.4270.

[6] J.M. Norman, M.C. Anderson, W.P. Kustas, A.N. French, J. Mecikalski and R. Torn, "Remote sensing of surface energy fluxes at 101-m pixel resolutions", Water Resources Research, 2003, vol. 39, Issue 8, pp. 1221-1232.

[7] R. Rivas and V. Caselles, "A simplified equation to estimate spatial reference evaporation from remote sensing-based surface temperature and local meteorological data", 2004, Remote Sensing of Environment, vol. 83, pp. 68-76.

[8] V. Venturini, S. Islam and L. Rodríguez, "Estimation of evaporative fraction and evapotranspiration from MODIS products using a complementary based model", Remote Sensing of Environment, 2008, vol. 112, pp. 132-141.

[9] M.S. Moran, T.R. Clarke, Y. Inoue and A. Vidal, "Estimating crop water deficit using the relation between surface-air temperature and spectral vegetation index", Remote Sensing of Environment, 1994, vol. 49, Issue 3, pp. 246-263.

[10] P.D. Colaizzi, E.M., Barnes, T.R. Clarke, C.Y. Choi, M. Peter, P.M. Waller, J. Haberland and M. Kostrzews, "Water Stress Detection Under High Frequency Sprinkler Irrigation with Water Deficit Index", Journal of Irrigation and Drainage Engineering. JANUARY/FEBRUARY 2003.

[11] L.E. Pertovt, R. Rivas, J. Schirmbeck, W.O.G. Coelho and L. Vives, "Análisis de condicionantes ambientales del estrés hídrico de la vegetación en el sur de Brasil mediante imágenes NOAA – AVHRR, Boletín Geológico y Minero, 2008, vol. 119 Issue 1, pp. 119-124.

[12] L.A. Mendez-Barroso, J. Garatuza-Payan and E.R. Vivoni E.R., "Quantifying water stress on wheat using remote sensing in the Yaqui Valley, Sonora, Mexico", Agricultural Water Management, 2008, vol. 95, Issue 6, pp. 725-736.

[13] D. Girolimetto and V. Venturini, "Water stress estimation from NDVI-Ts plot and the wet environment evapotranspiration", Advances in Remote Sensing, 2013, vol. 2, Issue 4, pp. 283-291.

[14] Z. Sun, Q. Wang, Z. Ouyang and Y.Yang, "Evaluation of a complementary based model for mapping land surface evapotranspiration", Hydrology and Earth System Sciences, 2012, vol. 9, pp. 3029-3062

[15] I.J. Barton, "A parameterization of the evaporation from nonsatured surfaces", Journal of Applied Meteorology, 1979, vol. 18, pp. 43-47.

[16] D. Chen, J. Huang and T. Jackson, "Vegetation water content estimation for corn and soybeans using spectral indices derived from MODIS near- and short-wave infrared bands", Remote Sensing of Environment, 2005, vol. 98, pp. 225-236

[17] C.H.B. Priestley and R.J. Taylor, "On the Assessment of Surface Heat Flux and Evaporation Using Large-Scale Parameters", Monthly Weather Review, 1972, vol. 100, pp. 81–92.

[18] R.J. Granger, "A complementary relationship approach for evaporation from nonsaturated surfaces", Journal of Hydrology, 1989, vol. 111, pp. 31-38.

[19] V. Venturini, L. Rodríguez and G. Bisht, "A comparison among different modified Priestley and Taylor's equations to calculate actual evapotranspiration with MODIS data", International Journal of Remote Sensing, 2011, vol. 32, pp. 1319-1338.

[20] E.R. Hunt, B.N. Rock and P.S. Nobel, "Measurement of leaf relative water content by infrared reflectance", Remote Sensing of Environment, 1987, vol. 22, pp. 429-435.

[21] B.C. Gao, "NDWI-A normalized difference water index for remote sensing of vegetation liquid water from space", Remote Sensing of Environment, 1996, vol. 58, pp. 257-266.

[22] J. Penuelas, J. Piñol, R. Ogaya and I. Filella, "Estimation of plant water concentration by the reflectance water index (R900/R970)", International Journal of Remote Sensing**,** 1997, vol. 18, pp. 2869-2875.

[23] P. Ceccato, S. Flasse, S. Tarantola, S. Jacquemoud, J.M. Gregoire, "Detecting vegetation leaf water content using reflectance in the optical domain", Remote Sensing of Environment, 2001, vol. 77, pp. 22-33.

[24] R. Fensholt and I. Sandholt, "Derivation of a shortwave infrared water stress index from MODIS near- and shortwave infrared data in a semiarid environment", Remote Sensing of Environment, 2003, vol. 87, pp. 111-121.

[25] D.A. Sims and J.A. Gamon, "Estimation of vegetation water content and photosynthetic tissue area from spectral reflectance: a comparison of indices based on liquid water and chlorophyll absorption", Remote Sensing of Environment, 2003, vol. 84, pp. 526-537.

[26] P.J. Zarco-Tejada, C.A Rueda and S.L. Ustin, "Water content estimation in vegetation with MODIS reflectance data and model inversion methods", Remote Sensing of Environment, 2003, vol. 85, pp. 109-124.

[27] M. Maki, M. Ishiahra and M., Tamura, "Estimation of leaf water status to monitor the risk of forest fires by using remotely sensed data", Remote Sensing of Environment, 2004, vol. 90, pp. 441-450.

[28] Y.B. Cheng, P.J. Zarco-Tejada, D. Riano, C.A Rueda and S.L. Ustin, "Estimating vegetation water content with hyperspectral data for different canopy scenarios: Relationships between AVIRIS and MODIS indexes", Remote Sensing of Environment, 2006, vol. 105, pp.354-366.

[29] M. Trombetti, D. Riano, M.A. Rubio, Y.B. Cheng and S.L. Ustin, "Multi-temporal vegetation canopy water content retrieval and interpretation using artificial neural networks for the continental USA", Remote Sensing of Environment, 2008, vol. 112, pp. 203-215.

[30] P. Ceccato, N. Gobron, S. Flasse, B. Pinty and S. Tarantola, "Designing a spectral index to estimate vegetation water content from remote sensing data: Part 1. Theoretical approach", Remote Sensing of Environment, 2002a, vol. 82, pp. 188-197.

[31] M.T. Yilmaz, Jr. E.R. Hunt, L.D. Goins, S.L Ustin, V.C. Vanderbilt and T.J. Jackson, "Vegetation water content during SMEX04 from ground data and Landsat 5 Thematic Mapper imagery", Remote Sensing of Environment, 2008, vol. 112, pp. 350-362.

[32] W.J. Shuttleworth, "Evaporation models in hydrology. In: Schmugge, T.J., André, J.C. (Eds.). Land Surface Evaporation: Measurement and Parameterization". Springer, New York, 1991, pp. 93-120.

[33] J.M. Lewis, "The story behind the Bowen ratio", Bulletin of the American Meteorological Society, 1995, vol. 76, pp. 2433-2443.

[34] V. Venturini, L. Rodríguez and G. Bisht, "A comparison among different modified Priestley and Taylor's equations to calculate actual evapotranspiration with MODIS data", International Journal of Remote Sensing, 2010, vol. 32, Issue 5, pp. 1319-1338.

[35] C.O. Justice, J.R.G. Townshend, E.F. Vermote, E. Masuoka, R.E. Wolfe, N. Saleous, D.P. Roy and J.T. Morisette, "An overview of MODIS Land data processing and product status", Remote Sensing of Environment, 2002, vol. 83, Issue 2-Jan, 3-15.

[36] E.F. Vermote, N.Z. Saleous and C.O. Justice, "Atmospheric correction of MODIS data in the visible to middle infrared: first results", Remote Sensing of Environment, 2002, vol. 83, Issue 2-Jan, pp. 97-111.

[37] W.P. Menzel, S.W. Seemann, J. Li and L.E. Gumley, "MODIS Atmospheric Profile Retrieval Algorithm Theoretical Basis Document", 2002, Version 6, Reference Number: ATBD-MOD-07. http://modis.gsfc.nasa.gov/data/atbd/atbd_mod07.pdf

[38] G. Bisht, V. Venturini, L. Jiang and S. Islam, "Estimation of net radiation using MODIS (Moderate Resolution Imaging Spectroradiometer) Terra Data for clear sky days", Remote Sensing of Environment, 2005, vol. 97, pp. 52-67.

[39] Z. Wan and J.A. Dozier, "A generalized split-window algorithm for retrieving land-surface temperature from space", IEEE Transactions on Geoscience and Remote Sensing, 1996, vol. 34, Issue 4, pp. 892-905.

[40] V. Venturini, G. Bisht, S. Islam and L. Jiang, "Comparison of evaporative fractions estimated from AVHRR and MODIS sensors over South Florida", Remote Sensing of Environment, 2004, vol. 93, pp. 77-86.

[41] P. Chavez, "Image based atmospheric corrections-revisited and improved", Photogrammetric Engineering and Remote Sensing, 1996, vol. 62, pp. 1025-1036.

[42] A.L. Buck, "New equations for computing vapor pressure and enhancement factor", Journal of Applied Meteorology, 1981, vol. 20, pp. 1527-1532.

[43] W.P. Kustas, J.M. Norman, M.C. Anderson and A.N. French, "Estimating sub-pixel surface temperature and energy fluxes from the vegetation index-radiometric temperature relationship", Remote Sensing of Environment, 2003, vol. 85, pp. 429-440.

[44] N. Batra, S. Islam, V. Venturini, G. Bisht and L. Jiang, "Estimation and Comparison of Evapotranspiration from MODIS and AVHRR sensors for Clear Sky Days over the southern Great Plains", 2006, Remote Sensing of Environment, vol. 103, pp. 1-15.

[45] J.D. Kalma, T.R. McVicar and M.F. McCabe, "Estimating Land Surface Evaporation: A Review of Methods Using Remotely Sensed Surface Temperature Data", Surveys in Geophysics, 2008, Vol. 29, Numbers 4-5, pp. 421-469

[46] D. Long and V.P. Singh, "A Two-source Trapezoid Model for Evapotranspiration (TTME) from satellite imagery", Remote Sensing of Environment, 2012, vol. 121, pp. 370-388.

[47] G.H. Hargreaves and Z.A. Samani, "Estimating of potential evapotranspiration", Journal of Irrigation and Drainage Engineering, 1982, E–ASCE 108, pp. 223-230.

[48] G.F. Makkink, "Testing the Penman formula by means of lysimeters", Journal of the Institution of Water Engineers, 1957, vol. 11, pp. 277-288.

[49] N.R. Patel, A.N. Mehta and A.M. Shekh, "Canopy temperature and water stress quantification in rainfed pigeonpea (Cajanus cajan (L.) Millsp.)", Agricultural and Forest Meteorology, 2001, vol. 109, pp. 223-232.